Benchmark calculations of nonconservative charged-particle swarms in dc electric and magnetic fields crossed at arbitrary angles

S. Dujko,[1,2,*] R. D. White,[1] Z. Lj. Petrović,[2] and R. E. Robson[1,3]
[1]*ARC Centre for Antimatter-Matter Studies, School of Engineering and Physical Science, James Cook University, Townsville, Queensland 4810, Australia*
[2]*Institute of Physics, University of Belgrade, P.O. Box 68, Zemun, Belgrade 11080, Serbia*
[3]*ARC Centre for Antimatter-Matter Studies, Research School of Physical Sciences, Australian National University, Canberra, Australian Capital Territory 2600, Australia*
(Received 4 January 2010; published 22 April 2010)

A multiterm solution of the Boltzmann equation has been developed and used to calculate transport coefficients of charged-particle swarms in gases under the influence of electric and magnetic fields crossed at arbitrary angles when nonconservative collisions are present. The hierarchy resulting from a spherical-harmonic decomposition of the Boltzmann equation in the hydrodynamic regime is solved numerically by representing the speed dependence of the phase-space distribution function in terms of an expansion in Sonine polynomials about a Maxwellian velocity distribution at an internally determined temperature. Results are given for electron swarms in certain collisional models for ionization and attachment over a range of angles between the fields and field strengths. The implicit and explicit effects of ionization and attachment on the electron-transport coefficients are considered using physical arguments. It is found that the difference between the two sets of transport coefficients, bulk and flux, resulting from the explicit effects of nonconservative collisions, can be controlled either by the variation in the magnetic field strengths or by the angles between the fields. In addition, it is shown that the phenomena of ionization cooling and/or attachment cooling/heating previously reported for dc electric fields carry over directly to the crossed electric and magnetic fields. The results of the Boltzmann equation analysis are compared with those obtained by a Monte Carlo simulation technique. The comparison confirms the theoretical basis and numerical integrity of the moment method for solving the Boltzmann equation and gives a set of well-established data that can be used to test future codes and plasma models.

DOI: 10.1103/PhysRevE.81.046403 PACS number(s): 52.25.Fi, 51.10.+y, 52.20.Fs, 52.25.Xz

I. INTRODUCTION

Studies of transport processes of charged-particle swarms in neutral gases in varying configurations of dc electric and magnetic fields have applications in diverse areas of science and technology ranging from swarm experiments used to determine electron- and ion-neutral interaction cross sections/potentials [1–5] to plasma processing [6,7], gas lasers [8], and drift chambers [9] used in high-energy physics. In plasma processing, large classes of plasma devices utilize magnetic fields with goal of enhancing plasma density or improving electron confinement. Examples include magnetrons (see, e.g., [10,11] and reference therein), Hall-effect-thruster discharges [12–14], inductively coupled plasma [15–19], neutral loop discharge plasma [20–23], magnetically enhanced parallel plate [24] and magnetically enhanced inductively coupled plasmas [25], electron cyclotron resonance sources, and helicon plasma discharges [25]. Although these devices operate in different geometries and different regimes, the common thread among these devices is a key role of magnetic field on both the electron heating mechanism and charged-particle species transport. A number of methods to treat this problem have been developed and have been applied to a variety of realistic multidimensional discharge configurations, e.g., the particle in cell/Monte Carlo collision technique, hybrid and fluid methods or kinetic models based on the Boltzmann equation. In particular, fluid models and/or fluid parts of hybrid models of such magnetized plasma discharges often require swarm transport coefficients as a function of electric and magnetic field strengths. As an illustrative example, in a recently developed two-dimensional hybrid model of a magnetron discharge [26,27] the low-energy electrons and ions in the collision-dominated bulk plasma region are treated using a fluid model while the fast nonequilibrium electrons in the cathode region are treated by a Monte Carlo simulation. The fluid part is based on the local-field approximation and requires the tabulation of electron-transport coefficients as a function of the reduced electric (E/n_0) and magnetic (B/n_0) fields and the angle ψ between the fields, where n_0 is the neutral number density. Other illustrative examples include the fluid modeling of electron transport in various magnetized plasma discharges carried out by Hagelaar [19,28] and two-dimensional time-dependent modeling of the collision-dominated ICP, based on the relaxation continuum theory developed at Keio University [16]. Both of these numerical models employ scaled transport coefficients in electric and magnetic fields, particularly those that describe the drift and diffusion normal to the direction defined by the electric field. Clearly, further advancements of such and similar fluid models are directly dependent on accurate modeling of charged particles transport in electric and magnetic fields, particularly under conditions where the angle between the fields varies and when the

*sasa.dujko@ipb.ac.rs

transport properties are significantly affected by the presence of nonconservative collisions. In addition to collisional nonequilibrium plasmas, a similar procedure and phenomenology may be employed to model various designs of gaseous detectors of elementary particles [9,29]. In this case it is even more important to have information on charged-particle transport in electric and magnetic fields at different angles as it affects the principle of operation even more directly [30]. This is the main avenue we explore in this work.

Studies of charged-particle swarm transport properties in spatially homogeneous electric and magnetic fields have been the subject of interest for a number of years. Both experimental and theoretical early works prior to 1980 on charged-particle swarms in electric and magnetic fields have been reviewed by Allis [31], Heylen [32], and Huxley and Crompton [33]. More recent results with particular emphasis on theoretical and numerical methods for solving the Boltzmann equation for charged-particle swarms in electric and magnetic fields have been reviewed by White *et al.* [34,35] while the application of a Monte Carlo simulation technique in the same field has been reviewed by Dujko *et al.* [36]. Other methods including path-integral methods [37,38] have also been applied. Experimental investigations of charged-particle swarms in electric and magnetic fields are rarely reported in the literature. To date, most of the experimental research for swarms in electric and magnetic fields has focused on designing and optimizing the drift chambers used in high-energy physics [39–41]. Of special note are the experimental investigations of Brennan and Garvie [42] under the steady-state Townsend conditions and those carried out at Heidelberg by Schmidt *et al.* [2,3]. The magnetic field was introduced in these experiments with the goal of: (i) refining the accuracy of low-energy scattering cross-section data and (ii) removing the lack of uniqueness in the determination of these cross sections. While the fluid plasma models require the transport coefficients as input data, kinetic models and/or kinetic segments of hybrid models of plasma discharges require good and reliable sets of cross sections.

The significant turning point in the development of the kinetic theory for charged-particle swarms in gases under the influence of electric and magnetic fields was the work of Ness [43], who presented a general formalism for solving the Boltzmann equation in the presence of nonconservative collisions. The formalism used was based on a spherical-harmonic expansion in velocity space of the charged-particle phase-space distribution function. In a subsequent paper [44], Ness expanded the speed (energy) dependence in terms of Sonine polynomials and thereby carried out the numerical solutions for electrons and light ions undergoing conservative collisions in a crossed field configuration. The formalism and software developed by Ness have been applied in a number of areas [44–46] and in particular were used to analyze the swarm data of the Heidelberg group [2,3]. In 1999, White *et al.* [47] extended the numerical solution of the conservative Boltzmann equation by: (i) considering the effects of the angle between the fields and (ii) representing the speed dependence of the phase-space distribution function in terms of an expansion in Sonine polynomials about a weighted sum of Maxwellian distributions at different temperatures (the so-called multi-Maxwellian expansion). The effect of the angle between the fields on both transport coefficients and distribution function and the inadequacies of expansions in terms of Legendre polynomials and effective-field approximations have been also addressed by White *et al.* [47–49]. In 2000, Ness and Makabe [50] extended the numerical solution to include ionization by electron impact, a nontrivial extension of the associated code. They considered the synergism of ionization processes and magnetic field on electron transport in pure argon. The calculated transport coefficients of Ness and Makabe (2000) have been used in modeling of an argon magnetron plasma [27]. The further extension of the numerical solution includes the recent work of White *et al.* who considered the electron-transport coefficients required for the modeling of bulk electron transport in an O_2 magnetron discharge. Considerable contributions have been also made by Li and Chen [8] and Loffhagen and Winkler [51] under conditions of spatially homogeneous number density. For swarms under nonhydrodynamic conditions when both the electric and magnetic fields are present, one ought to mention the recent works of Li *et al.* [52], Nicoletopoulos and Robson [53], and Winkler *et al.* [54]. Other theoretical and numerical methods have also been applied to this problem. These include the semiquantitative momentum-transfer theory [55,56] and Monte Carlo simulation [29,36,57–59]. The large and diverse literature associated with this type of problem has already been reviewed in [34,60,61] and will not be repeated here.

The aim of this paper is to present the systematic multiterm solution of the Boltzmann equation for spatially inhomogeneous charged-particle swarms in gases under the influence of spatially uniform electric and magnetic fields crossed at arbitrary angles to each other when nonconservative collisions are operative. In this paper, we extend previous work involving the Boltzmann equation on transport coefficient calculations in dc electric and magnetic fields crossed at arbitrary angle by considering the implicit and explicit effects of nonconservative collisions on the various transport properties. Following the previous work of White *et al.* [34,47], the starting point for the present discussion is a spherical harmonics decomposition of the Boltzmann equation and the hierarchy of kinetic equations derived by Ness [43]. In contrast to White *et al.* [47] who solved numerically Boltzmann's equation by representing the speed dependence of the phase-space distribution function in terms of an expansion in Sonine polynomials about a weighted sum of Maxwellian distributions at different temperatures, it is found in this work that for electron swarms the two-temperature method is generally sufficient with a single weighting Maxwellian. For a rigorous treatment of nonconservative collisions in varying configurations of electric and magnetic fields a second-order density gradient expansion of the distribution function was required. A nontrivial extension of the code for numerical solution of Boltzmann's equation has been made and calculations have been performed for special collisional models which involve nonconservative collisions. The results obtained by a multiterm theory for solving the Boltzmann equation are compared with those obtained by a Monte Carlo method, and hence the most comprehensive benchmark calculations of electron transport in electric and magnetic fields for arbitrary angles in the literature are made and presented in this work.

In Secs. II A and II B, we give a brief discussion of the theoretical multiterm solution of the Boltzmann equation and Monte Carlo simulation technique, respectively, under nonconservative conditions for arbitrary angles between electric and magnetic fields. In Sec. III, we present results of benchmarking. Transport properties are presented as a function of magnetic field strength and angle between the fields for certain model nonconservative gases. The variation and basic trends of behavior in the various transport properties with magnetic field strength and angle between the fields under nonconservative collisions are addressed using physical arguments.

II. THEORY

A. Multiterm solution of Boltzmann's equation

The behavior of charged-particle swarms in gases under the influence of electric and magnetic fields is described by the phase-space distribution function $f(\boldsymbol{r},\boldsymbol{v},t)$ representing the solution of the Boltzmann equation

$$\frac{\partial f}{\partial t}+\boldsymbol{c}\cdot\frac{\partial f}{\partial \boldsymbol{r}}+\frac{q}{m}[\boldsymbol{E}+\boldsymbol{c}\times\boldsymbol{B}]\cdot\frac{\partial f}{\partial \boldsymbol{c}}=-J(f,f_o), \tag{1}$$

where $\boldsymbol{r}$ and $\boldsymbol{c}$ denote the position and velocity coordinates while q and m are the charge and mass of the swarm particle and t is the time. The electric and magnetic fields are assumed to be spatially homogeneous with magnitudes E and B, respectively. In what follows, we employ a coordinate system in which $\boldsymbol{E}$ defines the z axis while $\boldsymbol{B}$ lies in the y-z plane, making an angle ψ with respect to the $\boldsymbol{E}$. Swarm conditions are assumed to apply where the charged-particle number density is much less than number density of neutral species and mutual interactions between swarm particles are negligible compared with swarm particle-neutral particle interactions. The right-hand side (RHS) of Eq. (1) denotes the linear charged-particle-neutral molecule collision operator, accounting for elastic, inelastic and nonconservative (e.g. ionizing and attaching) collisions. For elastic collisions we use the original Boltzmann collision operator [62], while for inelastic collisions we prefer the semiclassical generalization [63]. The attachment and ionization collision operators employed are detailed by Ness and Robson [64].

The theoretical foundations for solution Eq. (1) under nonconservative conditions and arbitrary angles were formulated by Ness [43]. The hierarchy of kinetic equations derived by Ness [43] has universal validity under hydrodynamic conditions and forms the starting point for the present investigation. In brief, the hierarchy is derived through a series of three expansions:

(i) the angular component of the velocity dependence of the phase-space distribution function f is represented in terms of an expansion in spherical harmonics,

$$f(\boldsymbol{r},\boldsymbol{c},t)=\sum_{l=0}^{\infty}\sum_{m=-l}^{l}f_m^{(l)}(\boldsymbol{r},c,t)Y_m^{[l]}(\hat{\boldsymbol{c}}), \tag{2}$$

where $Y_m^{[l]}(\hat{\boldsymbol{c}})$ are spherical harmonics and $\hat{\boldsymbol{c}}$ denotes the angles of $\boldsymbol{c}$;

(ii) under hydrodynamic conditions the spatial dependence of the coefficient $f_m^{(l)}(\boldsymbol{r},c,t)$ may be represented by an expansion in terms of powers of the gradient operator acting on $n(\boldsymbol{r},t)$, the number density of electrons,

$$f_m^{(l)}(\boldsymbol{r},c,t)=\sum_{s=0}^{\infty}\sum_{\lambda=0}^{\infty}\sum_{\mu=-\lambda}^{\lambda}f(lm|s\lambda\mu;c)G_{\mu}^{(s\lambda)}n(\boldsymbol{r},t), \tag{3}$$

where $G_{\mu}^{(s\lambda)}$ is the irreducible gradient tensor operator [65]; and

(iii) the speed distribution function is represented in terms of modified Sonine polynomials about a Maxwellian at a temperature T_b,

$$f(lm|s\lambda\mu;c)=\omega(\alpha,c)\sum_{\nu=0}^{\infty}F(\nu lm|s\lambda\nu;\alpha)R_{\nu l}(\alpha,c), \tag{4}$$

where

$$R_{\nu l}(\alpha c)=N_{\nu l}\left(\frac{\alpha c}{\sqrt{2}}\right)^{l}S_{l+1/2}^{(\nu)}\left(\frac{\alpha^2c^2}{2}\right), \tag{5}$$

$$\omega(\alpha,c)=\left(\frac{\alpha^2}{2\pi}\right)^{3/2}\exp\left\{-\frac{\alpha^2c^2}{2}\right\}, \tag{6}$$

$$\alpha^2=\frac{m}{kT_b}, \tag{7}$$

$$N_{\nu l}^2=\frac{2\pi^{3/2}\nu!}{\Gamma(\nu+l+3/2)}, \tag{8}$$

and $S_{l+1/2}^{(\nu)}(\alpha^2c^2/2)$ are Sonine polynomials.

Performing the appropriate "matrix element" operations allows the Boltzmann equation to be converted into a hierarchy of doubly infinite coupled complex matrix equations,

$$\begin{aligned}\sum_{\nu'=0}^{\infty}\sum_{l'=0}^{\infty}\sum_{m'=0}^{\infty}\Bigg[&(n_0J_{\nu\nu'}^{l}(\alpha)+R_a\delta_{\nu\nu'})\delta_{ll'}\delta_{mm'}\\&+i\frac{qE}{m}\alpha(l'm10|lm)\langle\nu l||K^{[1]}(\alpha)||\nu'l'\rangle\\&+\frac{qB}{m}\Bigg\{\sqrt{(l-m)(l+m+1)}\frac{\sin\psi}{2}\delta_{m'm+1}\\&-\sqrt{(l+m)(l-m+1)}\frac{\sin\psi}{2}\delta_{m'm-1}-im\cos\psi\delta_{m'm}\Bigg\}\\&\times\delta_{\nu\nu'}\delta_{ll'}-n_0J_{0\nu'}^{0}(\alpha)F(\nu lm|000)(1-\delta_{s0}\delta_{\lambda0}\delta_{\mu0})\\&\times\delta_{l'0}\delta_{m'0}\Bigg]F(\nu'l'm'|s\lambda\nu)=X(\nu lm|s\lambda\nu),\end{aligned} \tag{9}$$

where R_a is the net creation rate. The reduced matrix elements of the collision operator $J_{\nu\nu'}^{l}(\alpha)$ and velocity derivative $\langle\nu l||K^{[1]}(\alpha)||\nu'l'\rangle$ are defined by Eqs. (11) and (12) in [64] while $(l'm10|lm)$ is a Clebsch-Gordan coefficient. The explicit expressions for the RHS are given in [47] for the case of conservative collisions only. For the purpose of this paper, these expressions are further modified and extended to

consider the explicit influence of nonconservative collisions on the diagonal elements of the diffusion tensor and are given in Appendix A and in Ref. [61]. Solution of Eq. (9) is made by truncation of the ν and l indices to $\nu_{\max}$ and $l_{\max}$, respectively. These values are independently increased until the desired convergence is obtained. T_b is not equal to the neutral gas temperature (the two-temperature method) and is used as a free parameter to optimize the convergence. After truncation, we have a hierarchy of coupled complex equations. This sparse system of equations is solved using standard sparse inversion routines.

The net creation rate is given by

$$R_a = n_0 \sum_{\nu=0}^{\infty} J^0_{0\nu}(\alpha) F(\nu lm|000), \tag{10}$$

where the matrix elements of the collision matrix, $J^0_{0\nu}$, are nonzero only when ionization and/or attachment are operative. The eigenvalue nature of the spatially homogeneous member of the hierarchy ($(s,\lambda,\mu)=(0,0,0)$) for nonconservative processes has been previously discussed [43,44,65]. The spatially homogeneous member of hierarchies (9) and (10) constitute a nonlinear system of equations for the spatially homogeneous moments $F(\nu lm|000)$. This system is solved iteratively using the similar method initially developed by Ness and co-workers [34,43,50,66].

In the absence of nonconservative collisions, it is sufficient only to solve the members of the hierarchy up to first order in the density gradients to determine all quantities of interest. However, in order to investigate the explicit influence of nonconservative collisions on both the drift and diffusion a second-order density gradient is required and the following members of hierarchy (9) must be considered: $(s,\lambda,\mu)=(0,0,0)$, (1,1,0), (1,1,1), (2,0,0), (2,2,0), (2,2,1), and (2,2,2). The bulk drift velocity components are related to the calculated moments via

$$W_x = \frac{\sqrt{2}}{\alpha}\mathrm{Im}\{F(011|000;\alpha)\} - \sqrt{2}\sum_{\nu'=0}^{\infty} n_0 J^0_{0\nu'}\,\mathrm{Im}\{F(\nu'00|111;\alpha)\}, \tag{11}$$

$$W_y = \frac{\sqrt{2}}{\alpha}\mathrm{Re}\{F(01-1|000;\alpha)\} + \sqrt{2}\sum_{\nu'=0}^{\infty} n_0 J^0_{0\nu'}\,\mathrm{Re}\{F(\nu'00|111;\alpha)\}, \tag{12}$$

$$W_z = -\frac{1}{\alpha}\mathrm{Im}\{F(010|000;\alpha)\} + \sum_{\nu'=0}^{\infty} n_0 J^0_{0\nu'}\,\mathrm{Im}\{F(\nu'00|110;\alpha)\}, \tag{13}$$

and the bulk diagonal elements of the diffusion tensor are given by

$$D_{xx} = -\frac{1}{\alpha}[\mathrm{Re}\{F(011|111;\alpha)\} - \mathrm{Re}\{F(01-1|111;\alpha)\}] - \sum_{\nu'=0}^{\infty} n_0 J^0_{0\nu'}\left[\frac{1}{\sqrt{3}}F(\nu'00|200;\alpha) + \frac{1}{\sqrt{6}}F(\nu'00|220;\alpha) - \mathrm{Re}\{F(\nu'00|222;\alpha)\}\right], \tag{14}$$

$$D_{yy} = -\frac{1}{\alpha}[\mathrm{Re}\{F(011|111;\alpha)\} + \mathrm{Re}\{F(01-1|111;\alpha)\}] - \sum_{\nu'=0}^{\infty} n_0 J^0_{0\nu'}\left[\frac{1}{\sqrt{3}}F(\nu'00|200;\alpha) + \frac{1}{\sqrt{6}}F(\nu'00|220;\alpha) + \mathrm{Re}\{F(\nu'00|222;\alpha)\}\right], \tag{15}$$

$$D_{zz} = -\frac{1}{\alpha}F(010|110;\alpha) - \sum_{\nu'=0}^{\infty} n_0 J^0_{0\nu'}\left[\frac{1}{\sqrt{3}}F(\nu'00|200;\alpha) - \sqrt{\frac{2}{3}}F(\nu'00|220;\alpha)\right]. \tag{16}$$

The off-diagonal elements of the diffusion tensor, $D_1=D_{xy}+D_{yx}$, $D_2=D_{xz}+D_{zx}$, and $D_3=D_{yz}+D_{zy}$ are given by

$$D_1 = \frac{2}{\alpha}\left[\mathrm{Im}\{F(01-1|111;\alpha)\} + \sum_{\nu'=0}^{\infty} n_0 J^0_{0\nu'}(\alpha)2\,\mathrm{Im}\{F(\nu'00|222;\alpha)\}\right], \tag{17}$$

$$D_2 = \frac{\sqrt{2}}{\alpha}[\mathrm{Re}\{F(010|111;\alpha)\} - \mathrm{Re}\{F(01-1|110;\alpha)\}] - \sum_{\nu'=0}^{\infty} n_0 J^0_{0\nu'}(\alpha)2\,\mathrm{Re}\{F(\nu'00|221;\alpha)\}, \tag{18}$$

$$D_3 = \frac{\sqrt{2}}{\alpha}[\mathrm{Im}\{F(010|111;\alpha)\} - \mathrm{Im}\{F(01-1|110;\alpha)\}] - \sum_{\nu'=0}^{\infty} n_0 J^0_{0\nu'}(\alpha)2\,\mathrm{Im}\{F(\nu'00|221;\alpha)\}. \tag{19}$$

Note that the expressions for the individual off-diagonal elements of the diffusion tensor are not directly obtainable from the diffusion equation but rather must be obtained from the flux-gradient relation [47]. This is a result of the parity and symmetry properties imposed on the distribution function, independently of the configuration of electric and magnetic fields. As a consequence, the explicit effects of nonconservative collisions cannot be found for the individual off-diagonal elements of the diffusion tensor. In other words, one may calculate only the flux components of the individual off-diagonal elements of the diffusion tensor and only the

implicit effects of nonconservative collisions can be isolated. However, in a crossed field configuration, the off-diagonal elements of the diffusion tensor are usually reported as a sum, e.g., $D_2=D_{\mathrm{Hall}}=D_{xz}+D_{zx}$, which is the quantity appearing in the continuity equation. Reactive corrections can thus be found for the Hall diffusion coefficient only.

The terms involving the summations in the drift velocity components and diagonal elements of the diffusion tensor represent the explicit effects of nonconservative collisions while the reminder constitute the flux contribution. Note, $\mathrm{Re}\{\cdot\}$ and $\mathrm{Im}\{\cdot\}$, respectively, represent the real and imaginary parts of the moments. Other transport properties of interest for this work are defined in some of our previous publications [34,47,61].

B. Monte Carlo simulation technique

The Monte Carlo simulation technique for electron swarms under the influence of spatially homogeneous electric and magnetic fields crossed is discussed in our previous papers [36,59,60]. Rather than present a full review of the simulation technique, we highlight below some important points associated with the technique. In this work, Monte Carlo method is employed as a tool to confirm the numerical accuracy and integrity of a multiterm theory for solving the Boltzmann equation. For the purpose of benchmarking presented here, it is assumed that an electron swarm develops under the influence of spatially uniform electric and magnetic fields in an infinite space. At $t=0$, electrons are initially released from the origin according to Maxwellian velocity distribution with the mean starting energy of 1 eV. Electrons gain the energy from the external electric field and dissipate it through various types of collisions including elastic, inelastic, and nonconservative (ionization/attachment) collisions. Thermal motion of the background neutral particles is neglected, and all simulations are performed for the low space-charge limit according to the standard definition of charged-particle swarms.

In the present Monte Carlo code we follow the spatiotemporal evolution of each electron through time steps governed by the minimum of two relevant time constants: mean collision time and cyclotron period for the $\boldsymbol{E}\times\boldsymbol{B}$ field. These finite time steps are used to solve the integral equation for the collision probability in order to determine the time of the next collision. This can be done using either the null collision [67] or integration technique [68]. In our code, an upgraded version of the latter approach is employed. The number of time steps is determined in such a way as to optimize the performance of the Monte Carlo code without reducing the accuracy of the final results. All dynamic properties of each electron such as the position, velocity, and energy are updated between the collisions. The equations of motion are solved analytically and the reader is referred to [59,61] for their explicit form. Once the moment of the next collision is established, the nature of the collision is determined by using the relative probabilities of various collision types. The next critical step is an accurate treatment of electron collision dynamics. All electron scatterings for the model gases used are assumed to be isotropic regardless of the nature of specific processes or energy. Therefore, the change in direction of the electron velocity may be expressed by uniformly distributed scattering angle within the interval $[0,\pi]$ and by the azimuthal angle uniformly distributed within the interval $[0,2\pi]$. In case of nonconservative collisions, the following procedure was adopted. In an attachment collision the electron is consumed and another electron is randomly selected in its place from the ensemble of the remaining electrons. Thus number of test particles and statistical quality remain constant without affecting the average properties [69]. When an ionization collision occurs, however, the implemented procedure allows an increase in the number of electrons upon reaching the limit set by memory resource. When the memory limit is reached a random electron is removed, again without affecting the averaged properties [69]. Both of these procedures have been tested in great detail for swarms under the influence of an electric field only and found to be correct [58,69,70].

Another critical issue when considering the electron swarms in electric and magnetic fields when nonconservative collisions are operative is the simulation speed. In general, one needs to follow a large number of electrons to achieve a good statistics of the final results and also to make sure that the relaxation to the steady-state conditions has been achieved. When magnetic field dominates the collisions, the energy transfer between the swarm particles and background molecules is not efficient. As a consequence, the relaxation process of various transport properties is much slower comparing to an electric field only situation. In order to optimize the simulation speed in the presence of nonconservative collisions and when both the electric and magnetic fields are present, the present code has been improved in the following way. Usually simulations were started with a small number of electrons (typically 1×10^4) and after relaxation to the steady state the electron swarm has been scaled at fixed time intervals. The scaling factor is a flexible parameter but usually this parameter was set to 2 in our simulations. In other words, this technique is based on simple duplication of somewhat relaxed electrons which are later followed independently [70]. The new born electron has the same dynamic properties (coordinate, velocity, and energy) as the original one and both of these identical electrons that describe the same trajectory were followed. At the moment of the collision with the background particles these two identical electrons scatter into different directions and from that point their trajectories differ but their initial properties are closer to the relaxed swarm conditions. This technique [69] does not change the energy distribution and allows an improvement in statistics of sampled properties. Some tests of this procedure over a wide range of conditions including the electric and magnetic field strengths and gas types have been made and results of testing indicate its validity and numerical integrity. Similar but not identical techniques are developed by Nolan and co-workers under hydrodynamic conditions [71] and by Dyatko and Napartovich under steady-state Townsend conditions [72]. This technique should not be confused with the already-mentioned technique to scale up or scale down the number of particles [71–73] as that was so far implemented under relaxed conditions only. We have tested the technique of speeding up the relaxation [69] and have shown that it

does not affect the final results while speeding up the relaxation considerably.

Transport coefficients and other transport properties are determined after relaxation to the steady state. In Monte Carlo simulation, the *bulk* transport coefficients may be determined from the rate of changes of the appropriate averages of the positions of the swarm particles in the *configuration* space [36,58–60,71,74]. The number changing reaction rate is defined by

$$\omega^{(0)} = -\alpha = \frac{d}{dt}(\ln N), \tag{20}$$

the drift velocity by

$$\omega^{(1)} = \boldsymbol{W} = \frac{d}{dt}\langle \boldsymbol{r} \rangle, \tag{21}$$

and the diffusion tensor by

$$\omega^{(2)} = \boldsymbol{D} = \frac{1}{2}\frac{d}{dt}\langle \boldsymbol{r}^{\star}\boldsymbol{r}^{\star} \rangle, \tag{22}$$

where N is the total number of electrons at any time and $\boldsymbol{r}^{\star} = \boldsymbol{r} - \langle \boldsymbol{r} \rangle$. In the absence of nonconservative collisions, flux drift velocity components and diagonal elements of the diffusion tensor can be obtained by a direct sampling technique, e.g., [36,58–60],

$$W_i = \left\langle \frac{dr_i}{dt} \right\rangle, \tag{23}$$

$$D_{ii} = \langle r_i v_i \rangle - \langle r_i \rangle \langle v_i \rangle, \tag{24}$$

where v_i is the electron velocity and $i = x, y, z$.

III. RESULTS AND DISCUSSION

In this section we investigate the transport properties of an isolated swarm undergoing model ionization interactions in gases under the influence of electric and magnetic fields crossed at arbitrary angle. Attachment results are presented in Appendix B.

Ionization model of Lucas and Saelee

For the consideration of ionization processes on the electron-transport coefficients and properties, we consider the benchmark model of Lucas and Saelee [75]. The details of this model are

$$\sigma_{el}(\epsilon) = 4\epsilon^{-1/2} \ \text{Å}^2,$$

$$\sigma_{ex}(\epsilon) = \begin{cases} 0.1(1-F)(\epsilon - 15.6) \ \text{Å}^2, & \epsilon \geq 15.6 \ \text{eV} \\ 0, & \epsilon < 15.6 \ \text{eV} \end{cases},$$

$$\sigma_{I}(\epsilon) = \begin{cases} 0.1F(\epsilon - 15.6) \ \text{Å}^2, & \epsilon \geq 15.6 \ \text{eV} \\ 0, & \epsilon < 15.6 \ \text{eV} \end{cases},$$

$$P(q, \epsilon') = 1, \quad m/m_o = 10^{-3}, \quad E/n_o = 10 \ \text{Td}, \quad T_o = 0 \ \text{K}, \tag{25}$$

where σ_{el}, σ_{ex}, and σ_I represent the cross sections for elastic, inelastic, and ionization collisions, respectively. In the above cross-section definitions energy is in eV, T_0 is the temperature of the neutral gas molecules, while M and m denote the molecular and electron mass, respectively. The parameter F controls the magnitude of the excitation and ionization cross sections. All scattering events are assumed isotropic and the cross sections listed above are "total" cross sections, that is, integrated over all angles. The ionization partition function $P(q, \epsilon')$ (where q is the fraction of the available energy after ionization given to the ejected electron and ϵ' is incident energy) is set equal to unity implying that all the fractions $0 \leq q \leq 1$ are equiprobable. As Ness and Robson pointed out [64], for sufficiently weak electric fields, the ionization rates are low and hence the electron-transport properties are relatively insensitive to the magnitude of the partition function. Therefore, the above assumption is justified. Conversely, for high ionization rates, accurate knowledge of the partitioning of the available energy between the incident and ejected electrons is required. The sensitivity of the electron-transport coefficients to postionization energy partitioning has been studied using a Monte Carlo method [76] and multiterm theory for solving the Boltzmann equation [77].

Calculations have been made for a carefully selected set of input parameters. We consider the reduced electric field of 10 Td (1 Td$=10^{-21}$ Vm^2), the reduced magnetic field range: 100–1000 Hx (1 Hx$=10^{-27}$ Tm^3), and angles between 0 and $\pi/2$ rad. The symmetry properties outlined by White *et al.* [47] can be used to consider angles greater than $\pi/2$ rad. Calculations are performed for different values of F. If the model parameter F is set to zero, no ionization occurs. This gas model is then reduced to elastic and excitation cross sections where the number of particles is conserved. If the model parameter F is set to 0.5, the cross sections for ionization and excitation have the same magnitude, and finally if the model parameter F is set to unity, no excitation occurs. Thus, we use the ionization model of Lucas and Saelee to isolate and separate effects of inelastic and ionization collisions, respectively, without affecting the total cross section.

Independent of the parameter F, convergence to within 0.5% was achieved for $l_{\max}=2$, indicating that inelastic collisions had little effect on the anisotropy of the velocity distribution function. For this model, the two-term approximation ($l_{\max}=1$) however generally fails to provide the correct values for the diffusion coefficients. In all cases, agreement is very good within the statistical uncertainty of Monte Carlo results.

In Fig. 1 we show the variation in the mean energy ε with ψ for B/n_0 of 100, 200, and 1000 Hx at E/n_0 of 10 Td. In Fig. 1 one can immediately see that the results obtained by a multiterm theory for solving the Boltzmann equation indicate strong agreement with those obtained by a Monte Carlo simulation technique. The mean energy monotonically decreases with ψ and/or B/n_0 for all F. This is the well-known phenomenon of "magnetic cooling" and it results from an inability of the electric field to efficiently pump the energy

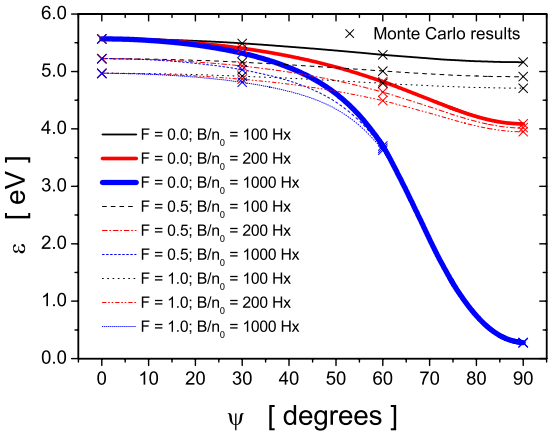

FIG. 1. (Color online) Variation in the mean energy as a function of B/n_0 and ψ for the ionization model of Lucas and Saelee. The solid lines represent the mean energies for $F=0$ while the other lines represent the mean energy for $F=0.5$ and $F=1$, as indicated on the graph. Monte Carlo results are given by symbol $\times$.

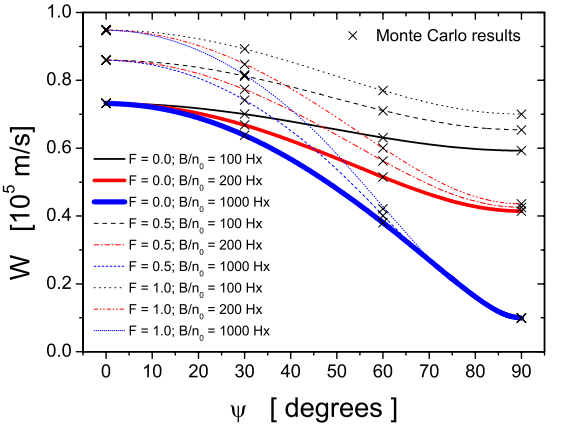

FIG. 3. (Color online) Variation in the drift speed as a function of B/n_0 and ψ for the ionization model of Lucas and Saelee. The solid lines represent the flux values while the other lines represent the bulk values for $F=0.5$ and $F=1$ as indicated on the graph. Monte Carlo results are given by symbol $\times$.

into the system [44] because the electrons change the direction of motion due to the magnetic field. This phenomenon is enhanced as the component of the magnetic field perpendicular to the electric field is increased. It is interesting to note that this phenomenon is generally independent of the gas considered and has been observed previously for all model [44,47,56] and real [36,49,59,66] gases. Only recently it has been shown that for a very narrow range of conditions the mean energy may begin to rise with the magnetic field [50]. In particular, for parallel fields ($\psi=0$), on average the electrons are traveling in the direction of the electric and magnetic field and hence the magnetic field has no explicit effect. Consequently the mean energy is independent of B/n_0.

In Fig. 1 we observe that mean energy decreases with increasing F for fixed B/n_0 and ψ in the collision-dominated regime. After an ionization process, the remaining energy is always shared between two electrons while in the case of inelastic collision, the remaining energy is held by only one electron. As a consequence, the mean energy after ionization is lower than that after inelastic collision, a phenomenon usually called energy dilution due to ionization [78]. The phenomenon of ionization cooling of the swarm is well known in dc electric fields and is shown in Fig. 1 to carry over directly to crossed dc electric and magnetic fields but only in the collision-dominated regime. As the angle between the fields increases for B/n_0 of 1000 Hx (magnetic field-controlled regime) this phenomenon is significantly reduced. The application of a magnetic field leads to the Maxwellization of high-energy electrons, and as a result the influence of both the excitation and ionization processes is significantly reduced. The reduction in the ionization rate for an increasing B/n_0 and/or ψ is clearly evident from Fig. 2.

For the ionization model of Lucas and Saelee, the drift speed is a one-to-one function of the mean energy, and hence the drift speed shows the same trends as the mean energy, as shown in Fig. 3. For this model, the implicit effect of ionization on the drift velocity is weak, and the flux components for $F=0.5$ and $F=1$ are essentially equal to the $F=0$ profile. Therefore, in Fig. 3 the flux component for $F=0$ is shown only. As B/n_0 and/or ψ increase, both the bulk and flux val-

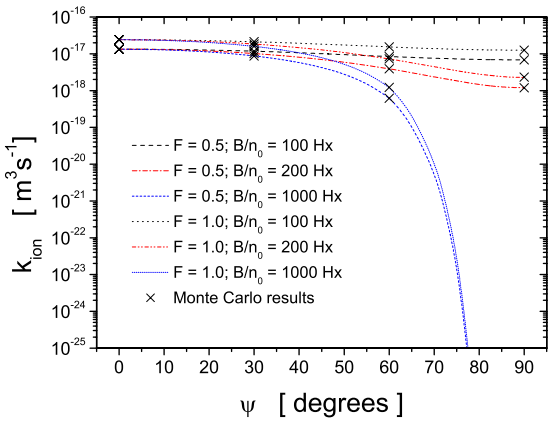

FIG. 2. (Color online) Variation in the ionization rate as a function of B/n_0 and ψ for the ionization model of Lucas and Saelee. Monte Carlo results are given by symbol $\times$.

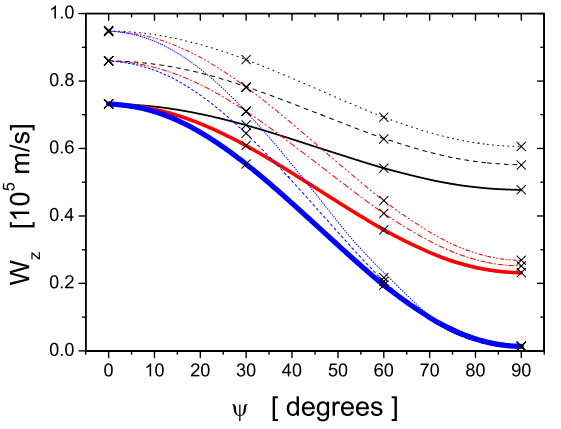

FIG. 4. (Color online) Variation in the z-drift velocity component as a function of B/n_0 and ψ for the ionization model of Lucas and Saelee for the same conditions as those in Fig. 3.

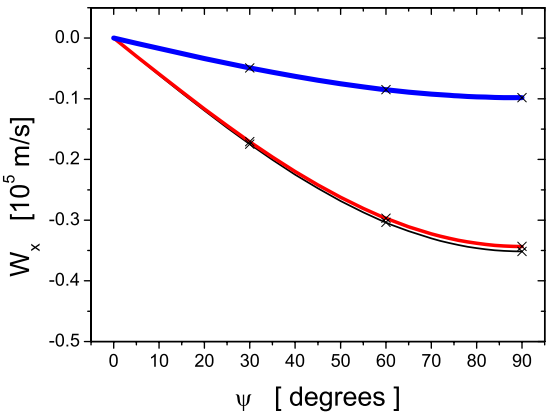

FIG. 5. (Color online) Variation in the flux x-drift velocity component as a function of B/n_0 and ψ for the ionization model of Lucas and Saelee for the same conditions as those in Fig. 3.

ues of the drift speed monotonically decrease. This is not a general rule; the exceptions are the gases which give rise to negative differential conductivity. Typical examples include methane [49,77,79] and carbon tetrafluoride [36,59].

The drift velocity components W_x and W_y satisfy the following symmetry properties [47]: $W_x=W_y=0$ for $\psi=0$ and $W_y=0$ for $\psi=90°$. In Fig. 4 we show the bulk and flux values of the drift velocity component along the z direction, while in Figs. 5 and 6 the drift velocity components along the x and y directions are shown. For clarity, in Fig. 5 we show only the flux values of W_x since there are no differences between flux and bulk components for this drift velocity component for all ψ considered [34,36,50,59]. We discuss this point further below. Two interesting properties are clearly evident from these profiles: (i) for an increasing ψ, W_x monotonically increases, W_y has a maximal property and W_z monotonically decreases; (ii) for a fixed angle between the fields ψ, the magnitudes of W_x, W_y, and W_z display respectively the maximal property, monotonically increase and monotonically decrease as B/n_0 is increased. These properties are quite general and have been previously observed for model [47] and real gases [59,66]. It is interesting to note that the flux W_y profiles follow the sin 2ψ dependence while the corresponding profiles of the bulk components are slightly shifted to the right, indicating the complex variation in the averaged energy along the swarm in the y direction. As expected, the deviations between the flux and bulk components of W_z are diminished as the angle ψ is increased for all B/n_0 considered. In particular, in the magnetic field-controlled regime (B/n_0 of 1000 Hx and $\psi>70°$) there are no differences between the bulk and flux components of both W_y and W_z. For the flux drift velocity components agreement with Monte Carlo results is within 0.5% while for the bulk the results agree to within 1% with those obtained by a Monte Carlo simulation. The same applies for the drift speed.

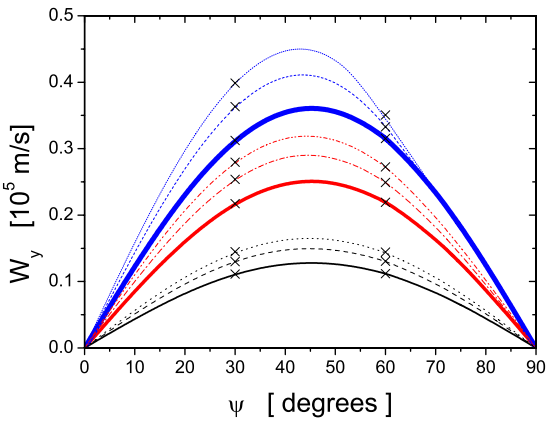

FIG. 6. (Color online) Variation in the y-drift velocity component as a function of B/n_0 and ψ for the ionization model of Lucas and Saelee for the same conditions as those in Fig. 3.

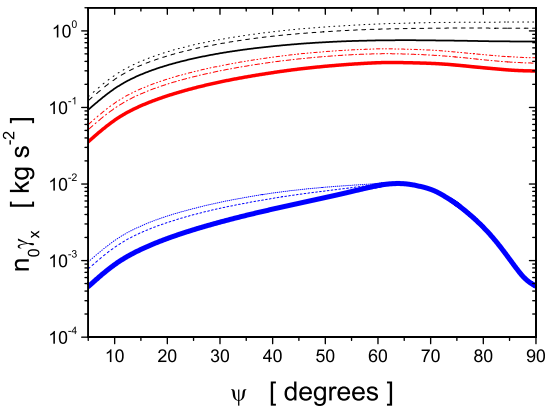

FIG. 7. (Color online) Variation in the x-component of the gradient energy vector as a function of B/n_0 and ψ for the ionization model of Lucas and Saelee for the same conditions as those in Fig. 1.

Let us consider now the origin of differences between the bulk and flux components of the drift velocity components. To study in detail the effect of nonconservative collisions on electron transport, we need to consider the spatial profile of the average energy through the swarm. As pointed out in [56], the gradient energy vector plays a key role in physical understanding of the effects of nonconservative collisions on electron-transport coefficients. For an arbitrary field configuration studied here, the gradient energy vector γ satisfies the

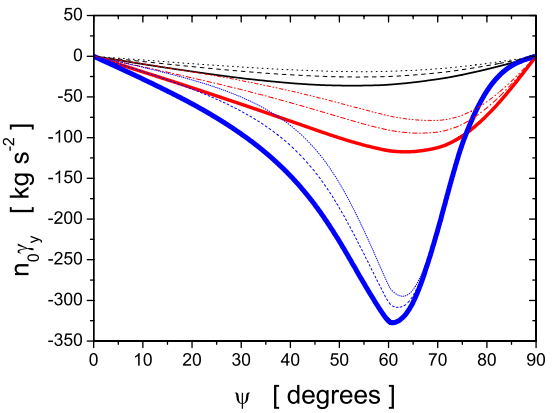

FIG. 8. (Color online) Variation in the y-component of the gradient energy vector as a function of B/n_0 and ψ for the ionization model of Lucas and Saelee for the same conditions as those in Fig. 1.

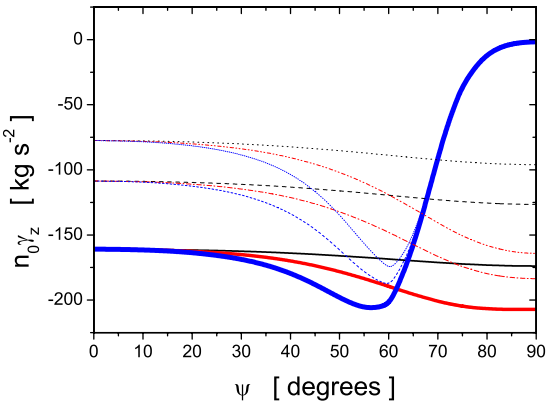

FIG. 9. (Color online) Variation in the y-component of the gradient energy vector as a function of B/n_0 and ψ for the ionization model of Lucas and Saelee for the same conditions as those in Fig. 1.

following symmetry conditions: $\gamma_x=\gamma_y=0$ for $\psi=0$ and $\gamma_y=0$ for $\psi=90°$. These symmetry properties are independent of the gas considered. In Figs. 7–9 we display the y and z, the gradient energy vector components as a function of B/n_0 and ψ. As can be observed, γ_y (see Fig. 8) displays a maximal property for all B/n_0 considered here with respect to ψ while γ_z (see Fig. 9) monotonically increases for B/n_0 of 100 and 200 Hx and displays a maximal property for B/n_0 of 1000 Hx. In the collision-dominated regime and for the angles up to $\psi=60°$, γ_y is an increasing function of B/n_0 and decreasing function of the parameter F. However, as ψ is further increased, there are no differences between the γ_y profiles for all F considered. Similar behavior can be observed in the profiles of γ_z but only for B/n_0 of 1000 Hx. Both γ_y and γ_z are negative (or zero) for all ψ, indicating the average energy increases through the swarm in these directions in the direction that the swarm is drifting.

In Fig. 7 we show the x component of the gradient energy vector γ_x, as a function of B/n_0 and ψ. We observe that in contrast to the y and z directions, there is a very little spatial variation in the average energy along the x axis ($\boldsymbol{E}\times\boldsymbol{B}$ direction). Further and in contrast to γ_y and γ_z, the spatial

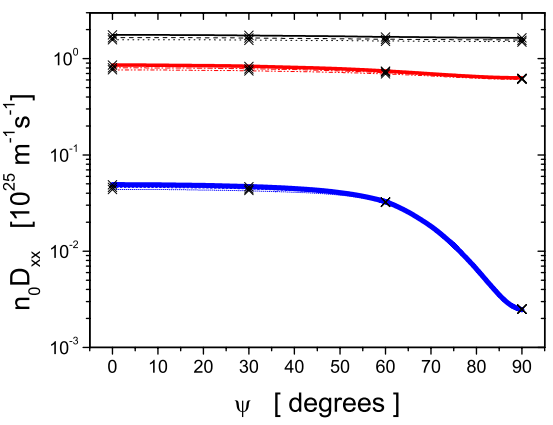

FIG. 10. (Color online) Variation in the D_{xx} as a function of B/n_0 and ψ for the ionization model of Lucas and Saelee for the same conditions as those in Fig. 1.

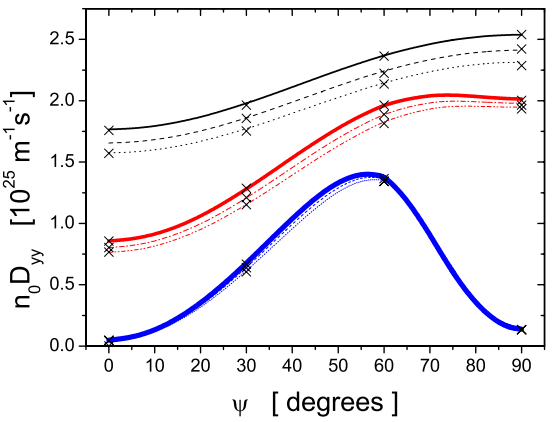

FIG. 11. (Color online) Variation in the D_{yy} as a function of B/n_0 and ψ for the ionization model of Lucas and Saelee for the same conditions as those in Fig. 1.

variation in the average energy in the $\boldsymbol{E}\times\boldsymbol{B}$ direction is in the opposite direction to the drift in that direction. This unexpected behavior of γ_x supports the previous works of Li *et al.* [56] and Dujko *et al.* [36,59].

Generally speaking, the distinction between flux and bulk components of the drift velocity vector elements is a consequence of spatially dependent nonconservative collisions resulting from a spatial variation of average electron energies within the swarm [64]. If the ionization rate is an increasing function of electron energy, electrons are preferentially created in regions of higher energy resulting in a shift in the centre of mass position as well as a modification of the spread about the centre of mass. For the ionization model of Lucas and Saelee and field configuration studied here, the electrons are preferentially created at the front of the swarm in the z direction and hence the magnitude of the bulk drift component in this direction is greater than the equivalent flux component. The same physical picture applies for drift in the y direction.

When we consider the drift velocity component along the $\boldsymbol{E}\times\boldsymbol{B}$ direction, the picture is not as simple. The drift velocity component along the $\boldsymbol{E}\times\boldsymbol{B}$ direction W_x appears in general to be less sensitive to the effects of ionization processes.

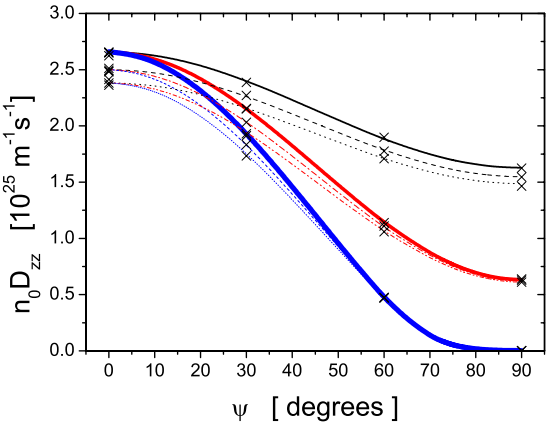

FIG. 12. (Color online) Variation in the D_{zz} as a function of B/n_0 and ψ for the ionization model of Lucas and Saelee for the same conditions as those in Fig. 1.

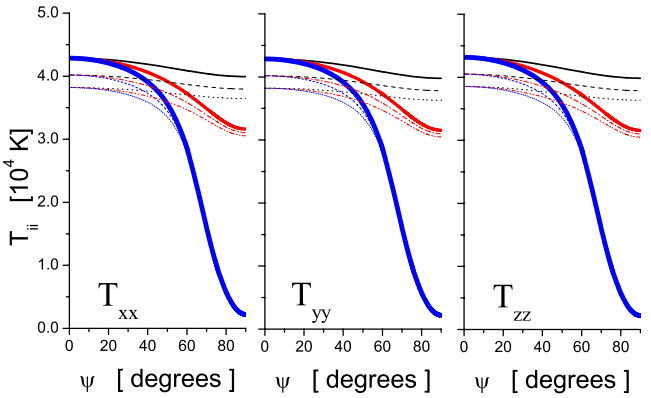

FIG. 13. (Color online) Variation in the diagonal elements of the temperature tensor as a function as a function of B/n_0 and ψ for the ionization model of Lucas and Saelee for the same conditions as those in Fig. 1.

This weak sensitivity of W_x to the ionization processes is indicative of an essentially symmetric spatial profile (with a slight bias) of average energy about the centre of mass of the swarm in the $\boldsymbol{E}\times\boldsymbol{B}$ direction. Consequently, the essentially symmetric production of electrons about the centre of mass by ionization process does not have a major impact on the position of the centroid, and the small differences between bulk and flux components in this direction then follow. These small differences are due to the slight nonsymmetrical bias in the spatial variation of the average energy in that direction. Further and in contrast to both the y and z directions, where the average energy increases in the direction of the drift in these directions (independent of the electric-field strength), in the x direction the spatial variation is dependent on the magnitude of the electric field. Recent studies on nonconservative electron transport in the presence of electric and magnetic fields for CF_4 using a Monte Carlo simulation technique [59] and for argon using a multiterm Boltzmann analysis [34] have revealed that for low E/n_0 the average energy decreases in the direction of the drift. Hence, for CF_4

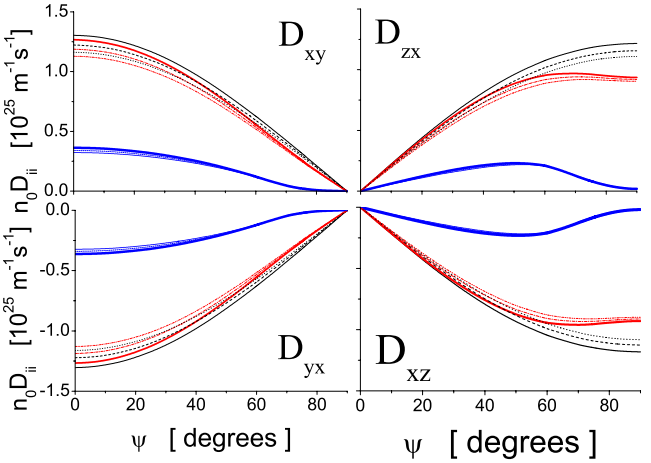

FIG. 14. (Color online) Variation in the of-diagonal elements of the diffusion tensor as a function as a function of B/n_0 and ψ for the ionization model of Lucas and Saelee for the same conditions as those in Fig. 1.

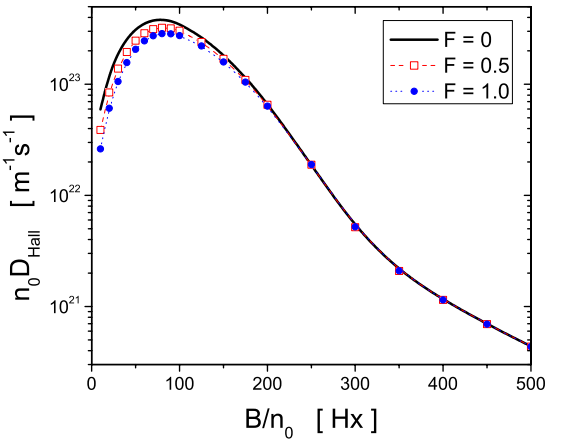

FIG. 15. (Color online) Variation in the flux Hall diffusion coefficient as a function of B/n_0 and parameter F for the ionization model of Lucas and Saelee.

at fields where attachment is the dominant nonconservative process, the bulk is greater than the flux while for argon due to the absence of attachment the opposite situation holds: the flux is greater than the bulk. In the case of CF_4, as E/n_0 increases and the ionization becomes dominant nonconservative process, there is a transition process where the flux is greater than bulk to the normal situation where the average energy increases in the direction of the drift and, consequently, the bulk is greater than the flux. It is important to note that this transition can be controlled by the angle between the fields. In any case, the synergism of large energy losses in inelastic collisions and strong influence of the ionization processes restore the regime where the bulk is greater than flux which is consistent with the other directions.

Figures 10–12 display the variation in the flux diagonal elements of the diffusion tensor with B/n_0 and ψ. In contrast to the drift velocity components, the implicit effects of the ionization processes on the diagonal elements of the diffusion tensor are quite strong, and hence we observe different profiles for different ionization degrees F. Due to the complexity and interplay of various factors which influence the

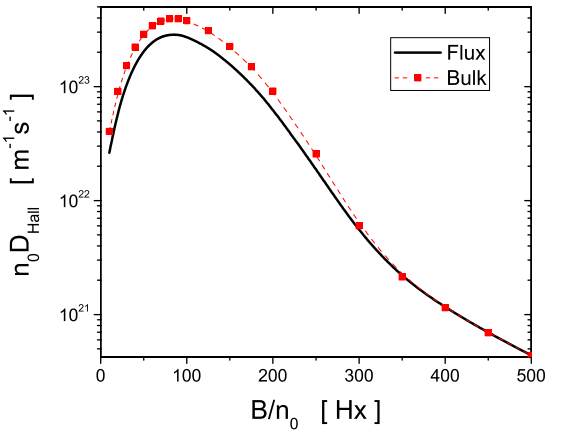

FIG. 16. (Color online) Variation in the flux and bulk Hall diffusion coefficient as a function of B/n_0 for the ionization model of Lucas and Saelee. The parameter F is set to 1.

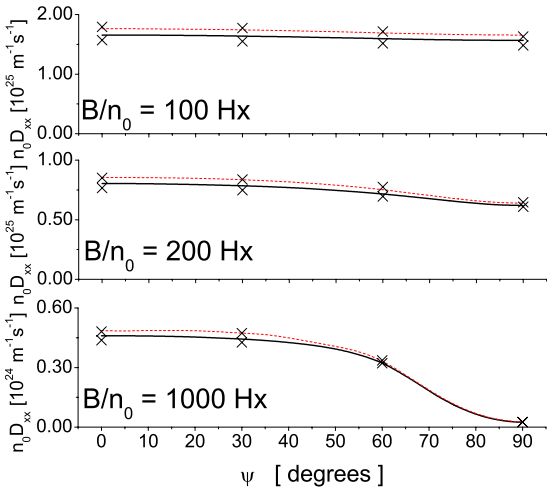

FIG. 17. (Color online) Variation in the bulk (dashed line) and flux (full line) values for D_{xx} as a function of B/n_0 and ψ for the ionization model of Lucas and Saelee. The parameter F is set to 1. The results obtained by a Monte Carlo simulation technique are presented by symbol $\times$.

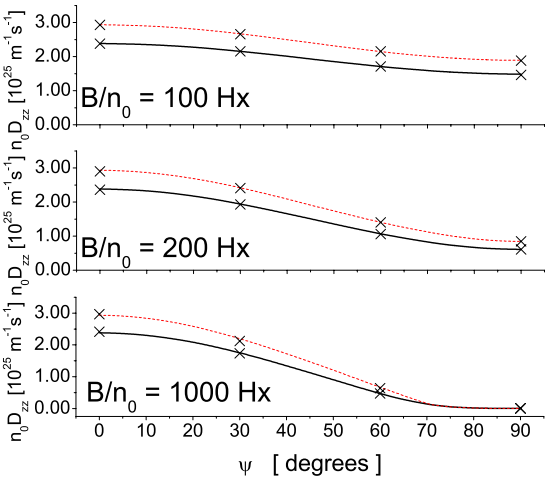

FIG. 19. (Color online) Variation in the bulk (dashed line) and flux (full line) values for D_{zz} as a function of B/n_0 and ψ for the ionization model of Lucas and Saelee. The parameter F is set to 1. The results obtained by a Monte Carlo simulation technique are presented by symbol $\times$.

diffusion tensor it is often hard to fully understand and elucidate even the basic trends in the profiles of the diffusion tensor components. These factors include: (a) the thermal anisotropy effect resulting from different random electron motion in different directions, (b) the magnetic anisotropy effect which acts to inhibit diffusion in the plane perpendicular to the magnetic field, and (c) the anisotropy induced by the electric field resulting from a spatial variation of the average energy and local average velocities throughout the swarm which act so as to either inhibit or enhance diffusion. In addition, to this triple anisotropy, the effects of collisions, energy-dependent total collision frequency, and couplings of these factors can further complicate the physical content of this issue. A convenient way to isolate and elucidate the phenomena associated only with the field effects is using a simple analytical form of cross sections in the calculations [47]. For the ionization model of Lucas and Saelee the electric-field-induced anisotropy is almost absent by virtue of the almost energy independent collision frequency. In addition, the thermal anisotropy is also significantly reduced indicating the fact that this model enables us to study the synergism of the anisotropy introduced by explicit orbital effects

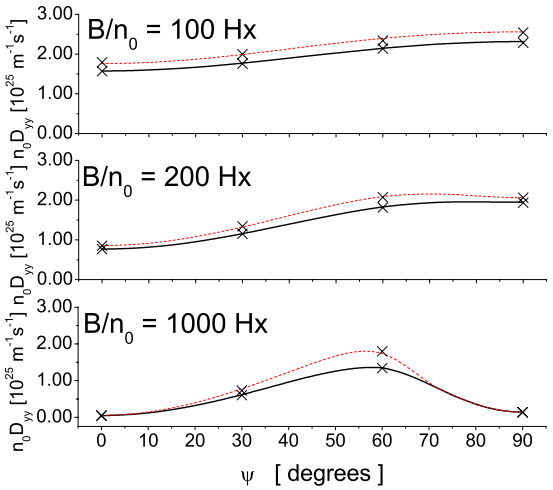

FIG. 18. (Color online) Variation in the bulk (dashed line) and flux (full line) values for D_{yy} as a function of B/n_0 and ψ for the ionization model of Lucas and Saelee. The parameter F is set to 1. The results obtained by a Monte Carlo simulation technique are presented by symbol $\times$.

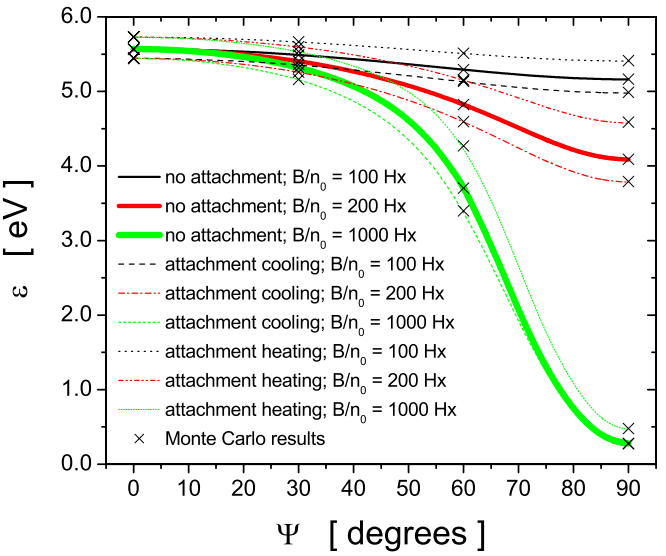

FIG. 20. (Color online) Variation in the mean energy as a function of B/n_0 and ψ for the modified attachment model of Ness and Robson. The solid lines represent the mean energies for conservative (no attachment) case while the other lines represent the mean energy for nonconservative cases when the attachment cross section is directly proportional to the electron velocity (attachment cooling: $p=0.5$, $a=0.5$) and when the electron attachment is inversely proportional to the electron energy (attachment heating: $p=-1$), as indicated on the graph. The results obtained by a Monte Carlo simulation technique are presented by symbol $\times$.

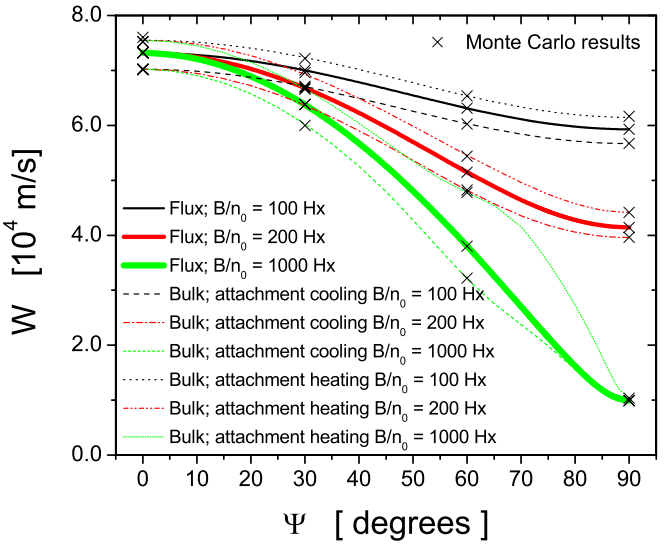

FIG. 21. (Color online) Variation in the drift speed as a function of B/n_0 and ψ for the modified attachment model of Ness and Robson. The solid lines represent the drift speed for conservative (no attachment) case (flux) while the other lines represent nonconservative cases when the attachment cross section is directly proportional to the electron velocity (attachment cooling: $p=0.5$, $a=0.5$) (bulk) and when the electron attachment is inversely proportional to the electron energy (attachment heating: $p=-1$) (bulk), as indicated on the graph. The results obtained by a Monte Carlo simulation technique are presented by symbol ×.

(the magnetic field anisotropy effect) and the effects of ionization processes. The previous study of [47] revealed some generic features of the diffusion tensor components which are again observed for the ionization model of Lucas and Saelee. We highlight these features and focus on a unique aspect for the ionization model of Lucas and Saelee and the explicit effects of nonconservative collisions on the diagonal diffusion tensor components.

From Figs. 10–12 we observe that for a fixed B/n_0, n_0D_{xx} and n_0D_{zz} are monotonically decreasing functions of ψ, while n_0D_{yy} displays a nonsymmetrical maximal property with ψ.

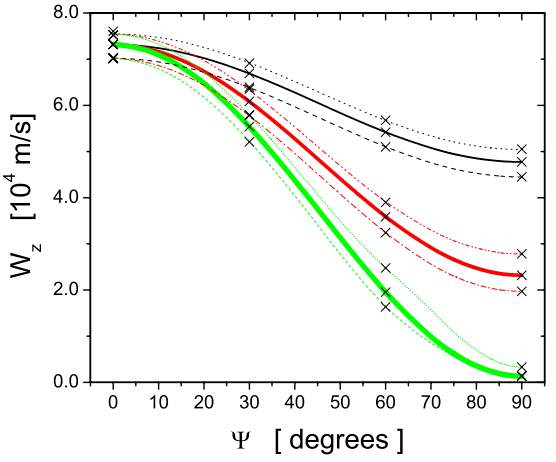

FIG. 22. (Color online) Variation in the W_z as a function of B/n_0 and ψ for the modified attachment model of Ness and Robson for the same conditions as those in Fig. 21

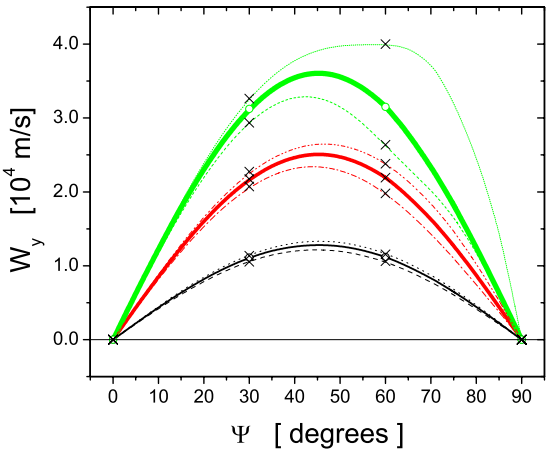

FIG. 23. (Color online) Variation in the W_y as a function of B/n_0 and ψ for the modified attachment model of Ness and Robson for the same conditions as those in Fig. 21

For a given ψ, we observe that both n_0D_{xx} and n_0D_{yy} are monotonically decreasing functions of B/n_0, as is n_0D_{zz} provided $\psi \neq 0$. For parallel fields ($\psi=0°$), the diffusion is isotropic in the plane perpendicular to $\boldsymbol{B}$, i.e. $n_0D_{xx}=n_0D_{yy}$ which can be expected from the symmetry properties [47]. In addition, for parallel field configuration n_0D_{zz} is independent of B/n_0 while n_0D_{xx} and n_0D_{yy} are monotonically decreasing functions of B/n_0. On the other hand, in a crossed field configuration ($\psi=90°$) and magnetic field dominated regime, the diffusion approaches isotropy in the plane perpendicular to $\boldsymbol{B}$. These are typical examples of the magnetic field anisotropy of the diffusion tensor.

The variation in the diagonal diffusion tensor elements with B/n_0 and ψ for the ionization model of Lucas and Saelee is predominantly induced by the thermal and magnetic field anisotropy effects. The thermal contribution is a decreasing function of both B/n_0 and ψ (see the components of the temperature tensor displayed in Fig. 13). On the other hand, the magnetic field acts to inhibit diffusion in a plane perpendicular to itself. This effect is further strengthened as the magnetic field is increased due to the fact that the elec-

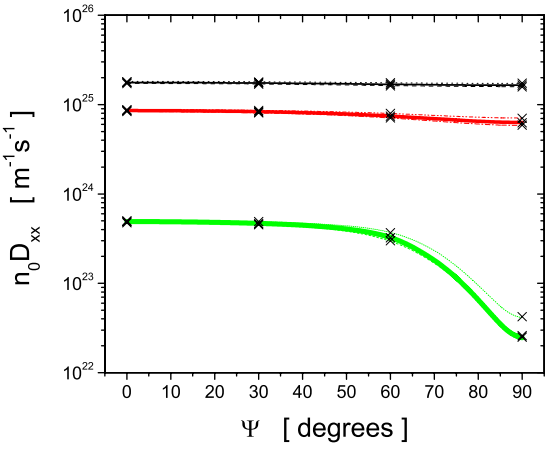

FIG. 24. (Color online) Variation in the flux n_0D_{xx} as a function of B/n_0 and ψ for the modified attachment model of Ness and Robson for the same conditions as those in Fig. 20

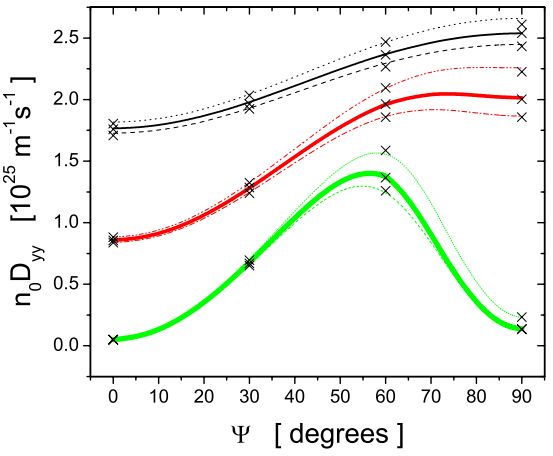

FIG. 25. (Color online) Variation in the flux $n_0 D_{yy}$ as a function of B/n_0 and ψ for the modified attachment model of Ness and Robson for the same conditions as those in Fig. 20

tron completes a greater fraction and number of orbits before undergoing a collision. Note that as B/n_0 increases, both D_{xx} and D_{zz} may vary over several orders of magnitude. While the inhibiting explicit orbital effect is strengthened with ψ for D_{zz}, the same effect is much less pronounced for D_{xx}. Consequently, D_{zz} monotonically and markedly decreases with ψ while D_{xx} is less sensitive to ψ. The diffusion coefficient D_{yy}, shown in Fig. 11 stands in contrast to both D_{xx} and D_{zz}. The variation in D_{yy} with B/n_0 is relatively small when compared to that for diffusion perpendicular to the magnetic field. The reason for this is that there is no explicit orbital effect on diffusion parallel to the magnetic field, and diffusion is purely thermal. For nonorthogonal field configurations, the variations in thermal and orbital effects with ψ tend to oppose each other, and hence $n_0 D_{yy}$ shows the maximal property with ψ.

In Fig. 14 we show the variation in the off-diagonal elements of the diffusion tensor as a function of B/n_0 and ψ for the ionization model of Lucas and Saelee. For illustrative purposes, D_{xy}, D_{zx}, D_{yx}, and D_{xz} are shown. The implicit

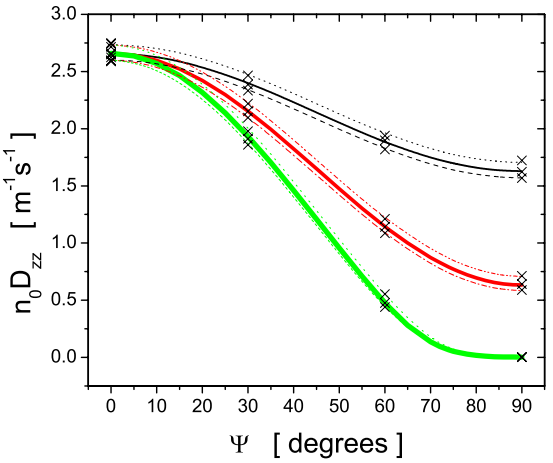

FIG. 26. (Color online) Variation in the flux $n_0 D_{zz}$ as a function of B/n_0 and ψ for the modified attachment model of Ness and Robson for the same conditions as those in Fig. 20

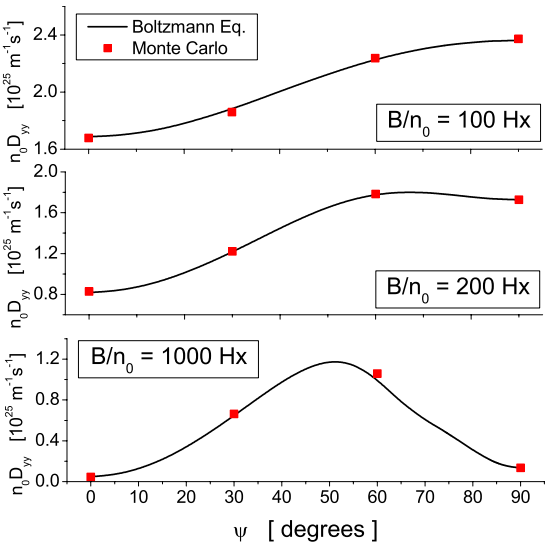

FIG. 27. (Color online) Variation in the bulk $n_0 D_{yy}$ as a function of B/n_0 and ψ for the modified attachment model of Ness and Robson when the attachment cross section is directly proportional to the electron velocity ($p=0.5$). The results obtained by a Monte Carlo simulation technique are presented by symbol $\times$.

effects of the ionization processes on the off-diagonal elements of the diffusion tensor are quite strong and hence different profiles for different ionization degrees F are clearly evident. The profiles are a monotonically decreasing function of the parameter F.

So physically, why do the off-diagonal elements of the diffusion tensor exist in electric and magnetic fields crossed at an arbitrary angle? Independently of the gas considered, the off-diagonal elements of the diffusion tensor arise from the interaction of the gradient-induced fluxes with the magnetic field. Consider, for example, orthogonal field configu-

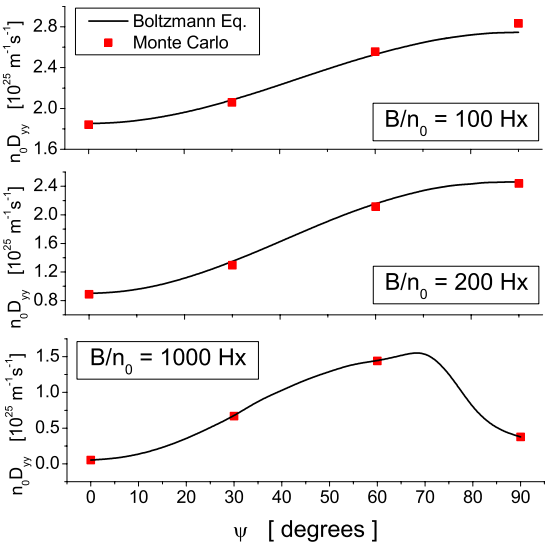

FIG. 28. (Color online) Variation in the bulk $n_0 D_{yy}$ as a function of B/n_0 and ψ for the modified attachment model of Ness and Robson when the electron attachment is inversely proportional to the electron energy ($p=-1$). The results obtained by a Monte Carlo simulation technique are presented by symbol $\times$.

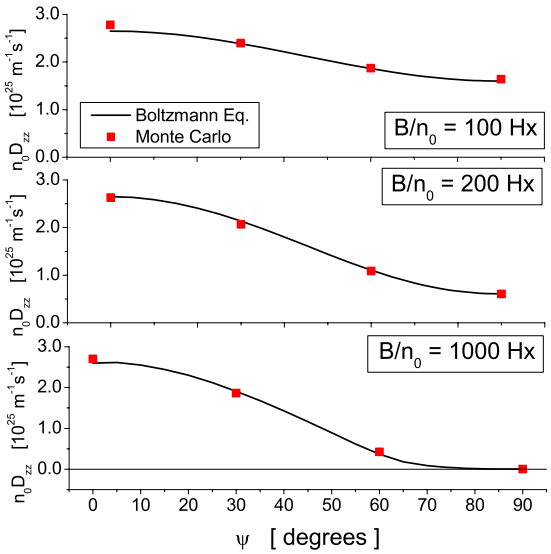

FIG. 29. (Color online) Variation in the bulk n_0D_{zz} as a function of B/n_0 and ψ for the modified attachment model of Ness and Robson when the attachment cross section is directly proportional to the electron velocity ($p=0.5$). The results obtained by a Monte Carlo simulation technique are presented by symbol $\times$.

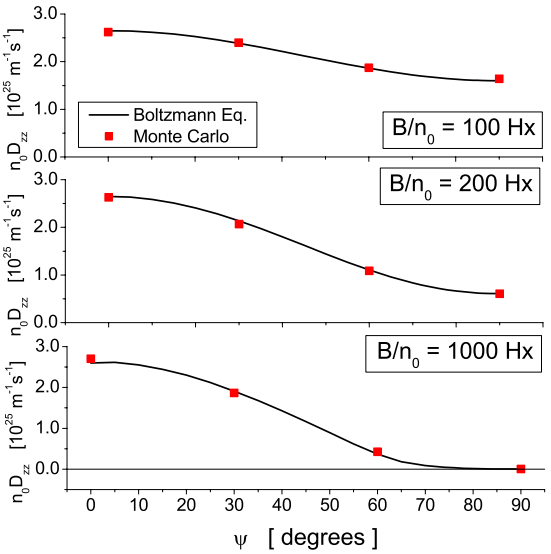

FIG. 30. (Color online) Variation in the bulk n_0D_{zz} as a function of B/n_0 and ψ for the modified attachment model of Ness and Robson when the electron attachment is inversely proportional to the electron energy ($p=-1$). The results obtained by a Monte Carlo simulation technique are presented by symbol $\times$.

ration. A density gradient in the x direction will cause a diffusive flux in the x direction. This flux could then interact with the magnetic field to again produce a flux in the z direction. Therefore, a gradient in the x direction can cause a flux in the x direction (described by D_{xx}) and the z direction (described by D_{zx}) but not one in the y direction. Hence for the orthogonal field configuration, symmetry properties follow and the coefficient D_{yx} is zero. These effects may be generally categorized as Hall currents, familiar in the plasma physics literature [44,47].

In Fig. 15 we display the variation in the flux Hall diffusion coefficient as a function of B/n_0 for all F considered. For the weak values of B/n_0, we observe different profiles for different ionization degrees F indicating a strong implicit effect of the ionization processes on this transport property. For an increasing B/n_0, however, these effects are significantly reduced. As can be observed, the Hall diffusion coefficient exhibits a nonsymmetrical profile, peaks at B/n_0 of around 80 Hx, and then decreases markedly. In fact, the Hall diffusion coefficient may vary over several orders of magnitude with B/n_0. The bulk and flux Hall diffusion coefficients for $F=1$ are shown in Fig. 16. The explicit effects of the ionization processes are obvious through the difference between the flux and bulk data.

In what follows the explicit influence of ionization on the diagonal elements of the diffusion tensor is analyzed by considering the difference between the bulk and flux values. In Figs. 17–19 we show the variation in the bulk and flux components of the diagonal elements of the diffusion tensor as a function of B/n_0 and ψ for the ionization model of Lucas and Saelee. For illustrative purposes, the parameter F is set to 1 to ensure the strongest effects of ionization. From Figs. 17–19 it is seen that differences between the bulk coefficients and their flux components can be greater than 25% and that the bulk is always greater than the corresponding flux components. The physical mechanism for this is discussed below. Similar but not identical trends have been recently observed for certain real gases in a crossed field configuration [59,66].

In contrast to the drift velocity components, the explicit effects of ionization on the diagonal elements of the diffusion tensor are dependent on both the first- and the second-order variations of the average energy through the swarm. As a consequence, there exists preferential creation of the electrons in certain directions if the ionization rate is energy dependent. This is the reason for the explicit modification of diffusion. The application of a magnetic field at arbitrary angle with respect to the electric field further modifies the spatial variation of the average energy profile, and in general both the first- and the second-order variations of the average energy are complex functions of B/n_0 and ψ. We may observe that the differences between the bulk and flux components for all diagonal diffusion elements are relatively insensitive with respect to the angle between the fields for low B/n_0. This is due to the small variations in the average energy along the swarm with ψ. However, if B/n_0 is increased, then the sensitivity of the difference between the bulk and flux values is greatly increased. It is interesting to note that various diagonal elements of the diffusion tensor show different sensitivities to the first- and second-order spatial variations in the average energy. As an illustrative example, the difference between the bulk and flux components for n_0D_{yy} and n_0D_{zz} can be associated with the first-order variation of the average energy (γ). However, as emphasized above, there is very little spatial variation in the average energy along the x axis. To understand the effect of ionization on n_0D_{xx} a comprehensive investigation of spatially dependent average energy and velocity is inevitable. In particular, the variation in the diffusive energy tensor associated with the second-order spatial variation in the average energy with

both B/n_0 and ψ must be studied. This is beyond the scope of this paper and we defer this to a future study.

IV. CONCLUSION

A multiterm theory for solving the spatially inhomogeneous Boltzmann equation has been developed to investigate the behavior of nonconservative charged-particle swarms in an unbounded neutral gas under the influence of spatially homogeneous electric and magnetic fields crossed at arbitrary angle. The numerical results for various transport coefficients obtained by a multiterm theory for solving the Boltzmann equation are presented for electron swarms in certain model gases and compared with those obtained by a Monte Carlo simulation technique. The excellent agreement between these two entirely independent techniques validates the theoretical basis and numerical integrity of the moment method for solving the Boltzmann equation and supports the application of the code in real gases. The duality in transport coefficients, the bulk and flux, arising from nonconservative collisions has been addressed, particularly for diffusion coefficients where similar studies are rare in the literature. The explicit and implicit effects of nonconservative collisions on the diagonal elements of the diffusion tensor are investigated by going to second order in the density gradient expansion. When considering the effects of nonconservative collisions on the off-diagonal elements of the diffusion tensor, it was shown that only the implicit effects can be isolated due to the parity and symmetry properties imposed on the distribution function. In particular, the bulk corrections of the Hall diffusion coefficient in a crossed field configuration have been highlighted. As for the drift velocity components, it was shown that the explicit and implicit effects of nonconservative collisions on the diffusion coefficients can be controlled either by the variation of the magnetic field strengths or by the angles between the fields. In general, knowledge of electron-transport coefficients and in particular the values of electric and magnetic field strengths and angles between the fields for which nonconservative collisions (attachment/ionization) may or may not have a significant effect on the drift and diffusion properties will be important for the operation or control of magnetically assisted plasma devices. In that respect, although this study was performed in the swarm limit, it provides a benchmark for plasma models in the limit of low electron density [80].

ACKNOWLEDGMENTS

All of the authors would like to acknowledge the support of the Australian Research Council and the Centre for Antimatter-Matter studies. Two of the authors (S.D. and Z.Lj.P.) were partly funded by the MNTR Project No. 141025. It is a pleasure to acknowledge the helpful discussions with K. F. Ness and Z. M. Raspopović.

APPENDIX A: THE EXPLICIT FORM OF THE RHS EQUATIONS

In this appendix we present the explicit expressions for the RHS of a hierarchy of doubly infinite coupled complex matrix Eq. (21). The general expression is given by

$$
\begin{aligned}
&X(\nu lm|s\lambda\mu;\alpha)\\
&=\sum_{\nu'=0}^{\infty}\sum_{l'=0}^{\infty}\sum_{m'=-l'}^{l'}\Bigg[-\frac{1}{\alpha}\sum_{\lambda_1=0}^{s-1}\sum_{\bar{\mu}=-1}^{1}(l'm'1\bar{\mu}|lm)(l'm'1\bar{\mu}|lm)(1\bar{\mu}\lambda_1\mu-\bar{\mu}|\lambda\mu)\langle\nu l||\alpha(t)c^{[1]}||\nu' l\rangle F(\nu l'm'|s-1\lambda_1\mu-\bar{\mu};\alpha)\\
&-\sum_{s_1=0}^{s}\sum_{\lambda_1=0}^{s_1}\sum_{\mu_1=-\lambda_1}^{\lambda_1}\sum_{\lambda_2=0}^{s-s_1}\sum_{\mu_2=-\lambda_2}^{\lambda_2}(\lambda_1\mu_1\lambda_2\mu_2|\lambda\mu)\omega(s-s_1\lambda_2\mu_2)(1-\delta_{ss_1}\delta_{\lambda_2 0}\delta_{\mu_2 0})(1-\delta_{s_1 0}\delta_{\lambda_1 0}\delta_{\mu_1 0})\\
&\times F(\nu' l'm'|s_1\lambda_1\mu_1;\alpha)\delta_{\nu\nu'}\delta_{ll'}\delta_{mm'}\\
&-\sum_{\lambda_1=0}^{s-1}\sum_{\bar{\mu}=-1}^{1}\frac{(-1)^{\bar{\mu}}}{\alpha(t)}(1\bar{\mu}\lambda_1\mu-\bar{\mu}|\lambda\mu)F(01-\bar{\mu}|s-1\lambda_1\mu-\bar{\mu};\alpha)F(\nu' l'm'|000;\alpha)(1-\delta_{s0}\delta_{\lambda 0}\delta_{\mu 0})\delta_{\nu\nu'}\delta_{ll'}\delta_{mm'}\Bigg],
\end{aligned}
\tag{A1}
$$

where the reduced matrix elements of velocity are given by Eq. (12a) of Ref. [64]. The expansion coefficients $\omega(s\lambda\nu)$ are given by

$$
\omega(s\lambda\mu;\alpha)=\frac{1}{\alpha}\sum_{\bar{\mu}=-1}^{1}\sum_{\lambda_1=0}^{s-1}(-1)^{\bar{\mu}}(1\bar{\mu}\lambda_1\mu-\bar{\mu}|\lambda\mu)F(01-\bar{\mu}|s-1\lambda_1\mu-\bar{\mu};\alpha)-n_0\sum_{\nu'=0}^{\infty}J^0_{0\nu'}(\alpha)F(\nu'00|s\lambda\mu;\alpha),
\tag{A2}
$$

where $J^0_{0\nu'}(\alpha)$ denotes the nonconservative part of the collision operator. Using the fundamental properties of the Clebsch-Gordon coefficients (see for example Ref. [81]), the following explicit general expression for the RHS of a hierarchy of kinetic equations and first order in density gradient (19) follows

$$X(\nu lm|11\mu;\alpha) = -\frac{1}{\alpha}\sum_{\nu'=0}^{\infty}\sum_{l'=0}^{\infty}[(l'm-\mu 1\mu|lm)\langle \nu l||\alpha c^{[1]}||\nu' l\rangle F(\nu' l' m-\mu|000;\alpha)] - \frac{(-1)^{\mu}}{\alpha}F(01-\mu|000;\alpha)F(\nu lm|000;\alpha). \tag{A3}$$

Similarly, the explicit expressions for the RHS and second order in the density gradients are given by

$$X(\nu lm|200;\alpha) = -\frac{1}{\alpha}\sum_{\nu'=0}^{\infty}\sum_{l'=0}^{\infty}\sum_{\bar{\mu}=-1}^{1}\left[(l'm-\bar{\mu}1\bar{\mu}|lm)\frac{(-1)^{1-\bar{\mu}}}{\sqrt{3}}\langle \nu l||\alpha c^{[1]}||\nu' l\rangle F(\nu' l' m-\bar{\mu}|11-\bar{\mu};\alpha)\right]$$
$$-\sum_{\bar{\mu}=-1}^{1}\frac{(-1)^{1+\bar{\mu}}}{\sqrt{3}}\omega(11\bar{\mu})F(\nu lm|11-\bar{\mu};\alpha) + \frac{1}{\alpha}\sum_{\bar{\mu}=-1}^{1}\frac{1}{\sqrt{3}}F(01-\bar{\mu}|11-\bar{\mu};\alpha)F(\nu lm|000;\alpha), \tag{A4}$$

$$X(\nu lm|22\mu;\alpha) = -\frac{1}{\alpha}\sum_{\nu'=0}^{\infty}\sum_{l'=0}^{\infty}\sum_{\bar{\mu}=-1}^{1}[(l'm-\bar{\mu}1\bar{\mu}|lm)(1\bar{\mu}1\mu-\bar{\mu}|2\mu)\langle \nu l||\alpha c^{[1]}||\nu' l\rangle F(\nu' l' m-\bar{\mu}|11\mu-\bar{\mu};\alpha)]$$
$$-\sum_{\bar{\mu}=-1}^{1}(1\mu-\bar{\mu}1\bar{\mu}|2\mu)\omega(11\bar{\mu})F(\nu lm|11\mu-\bar{\mu};\alpha)$$
$$-\sum_{\bar{\mu}=-1}^{1}\frac{(-1)^{\bar{\mu}}}{\alpha}(1\bar{\mu}1\mu-\bar{\mu}|2\mu)F(01-\bar{\mu}|11\mu-\bar{\mu};\alpha)F(\nu lm|000;\alpha). \tag{A5}$$

APPENDIX B: BENCHMARK RESULTS FOR THE MODIFIED ATTACHMENT MODEL OF NESS AND ROBSON

To test the multiterm theory for solving the Boltzmann equation outlined in Sec. II when electron attachment is present, in this appendix we present benchmark results for modified attachment model of Ness and Robson [64]. The details of this model are

$$\sigma_{el}(\epsilon) = 4\epsilon^{-1/2}\ \text{Å}^2,$$

$$\sigma_{ex}(\epsilon) = \begin{cases} 0.1(\epsilon-15.6)\ \text{Å}^2, & \epsilon \geq 15.6\ \text{eV} \\ 0, & \epsilon < 15.6\ \text{eV} \end{cases},$$

$$\sigma_a(\epsilon) = a\epsilon^p, \quad m/m_o = 10^{-3}, \quad E/n_o = 10\ \text{Td}, \quad T_o = 0\ \text{K}, \tag{B1}$$

where σ_{el}, σ_{ex}, and σ_a represent the cross sections for elastic, inelastic, and attachment, respectively. In the above cross-section definitions energy is in eV, T_0 is the temperature of the neutral gas molecules, while M and m denote the molecular and electron mass respectively. The parameter a determines the magnitude while the parameter p determines the energy dependence of the attachment cross section. This paper considers $p=0.5,-0.5,-1$, that is, case studies of attachment cross sections directly proportional to the electron velocity, inversely proportional to the electron velocity, and inversely proportional to the electron energy. When employing the attachment cross section directly proportional to the electron velocity, we consider $a=0.5$. Since inelastic collisions play an important role in this model, independent of the power p and attachment amplitude a, convergence was achieved in for $l_{\max}=2$. As pointed out by Ness and Robson [64], attachment has little effect on the isotropy of the velocity distribution function. The anisotropy of the velocity distribution function is induced by an active role of inelastic collisions and hence the two-term approximation generally fails for this model. It has been observed that diffusion coefficients are the most sensitive to the variation of the l index. The deviations between diffusion coefficients between the two- and three-term calculations could be up to 20%.

Another important aspect for this model is the case $p=-0.5$, where the attachment collision frequency is independent of energy. For such a power law, all bulk transport coefficients (aside from the attachment rate) were found to be independent of the attachment amplitude and equal to the corresponding flux values. This supports the numerical integrity of the present code in the presence of attachment collisions. For clarity, the electron-transport properties for this particular case will not be shown and explicitly labeled.

The results of benchmarking are displayed in Figs. 20–30. The physical properties can be understood from the suitable adaptation of those considered in Sec. III and for this reason only the results are presented in the Appendixes A and B. The results are in excellent agreement with those obtained by a Monte Carlo simulation technique.

[1] R. W. Crompton, Adv. At., Mol., Opt. Phys. **32**, 97 (1994).
[2] B. Schmidt, Comments At. Mol. Phys. **28**, 379 (1993).
[3] B. Schmidt, K. Berkhan, B. Gotz, and M. Muller, Phys. Scr. **T53**, 30 (1994).
[4] Z. Lj. Petrović, M. Šuvakov, Ž. Nikitović, S. Dujko, O. Šašić, J. Jovanović, G. Malović, and V. Stojanović, Plasma Sources Sci. Technol. **16**, S1 (2007).
[5] Z. Lj. Petrović, S. Dujko, D. Marić, G. Malović, Ž. Nikitović, O. Šašić, J. Jovanović, V. Stojanović, and M. Radmilović-Radjenović, J. Phys. D **42**, 194002 (2009).
[6] T. Makabe and Z. Lj. Petrović, *Plasma Electronics: Applications in Microelectronic Device Fabrication* (Taylor & Francis Group, New York, 2006).
[7] M. A. Liebermann and A. J. Lichtenberg, *Principles of Plasma Discharges and Materials Processing* (Wiley, New York, 1994).
[8] J. Li and Q. M. Chen, J. Phys. D **26**, 1541 (1993).
[9] W. Blum and L. Rolandi, *Particle Detection with Drift Chambers* (Springer, Berlin, 1993).
[10] K. Nanbu, K. Mitsui, and S. Kondo, J. Phys. D **33**, 2274 (2000).
[11] C. H. Shon and J. K. Lee, Appl. Surf. Sci. **192**, 258 (2002).
[12] L. Garrigues, A. Heron, J. C. Adam, and J. P. Boeuf, Plasma Sources Sci. Technol. **9**, 219 (2000).
[13] V. Latocha, L. Garrigues, P. Degond, and J. P. Boeuf, Plasma Sources Sci. Technol. **11**, 104 (2002).
[14] F. Taccogna, R. Schneider, S. Longo, and M. Capitelli, Plasma Sources Sci. Technol. **17**, 024003 (2008).
[15] M. Tadokoro, H. Hirata, N. Nakano, Z. Lj. Petrović, and T. Makabe, Phys. Rev. E **57**, R43 (1998).
[16] K. Kamimura, K. Iyanagi, N. Nakano, and T. Makabe, Jpn. J. Appl. Phys. **38**, 4429 (1999).
[17] V. A. Godyak, B. M. Alexandrovich, and V. I. Kolobov, Phys. Rev. E **64**, 026406 (2001).
[18] A. V. Vasenkov and M. J. Kushner, Phys. Rev. E **66**, 066411 (2002).
[19] G. J. M. Hagelaar, Phys. Rev. Lett. **100**, 025001 (2008).
[20] H. Tsuboi, M. Itoh, M. Tanabe, T. Hayashi, and T. Uchida, Jpn. J. Appl. Phys. **34**, 2476 (1995).
[21] D. O. O'Connell, D. L. Crintea, T. Gans, and U. Czarnetzki, Plasma Sources Sci. Technol. **16**, 543 (2007).
[22] D. O. O'Connell, T. Gans, D. L. Crintea, U. Czarnetzki, and N. Sadeghi, Plasma Sources Sci. Technol. **17**, 024022 (2008).
[23] H. Sugawara and Y. Sakai, J. Phys. D **41**, 135208 (2008).
[24] M. J. Kushner, J. Appl. Phys. **94**, 1436 (2003).
[25] R. L. Kinder and M. J. Kushner, J. Appl. Phys. **90**, 3699 (2001).
[26] E. Shidoji, H. Ohtake, N. Nakano, and T. Makabe, Jpn. J. Appl. Phys. **38**, 2131 (1999).
[27] E. Shidoji, K. F. Ness, and T. Makabe, Vacuum **60**, 299 (2001).
[28] G. J. M. Hagelaar, Plasma Sources Sci. Technol. **16**, S57 (2007).
[29] S. F. Biagi, Nucl. Instrum. Methods Phys. Res. A **421**, 234 (1999).
[30] P. Fonte, in Proceedings of the XXIX International Conference on the Phenomena in Ionized Gases (Cancun, Mexico) (2009).
[31] W. P. Allis, in *The Encyclopedia of Physics*, edited by S. Flugge (Springer, Berlin, 1956), Vol. XXI, p. 383.
[32] A. E. D. Heylen, IEE Proc., Part A: Phys. Sci., Meas. Instrum., Manage. Educ. **127**, 221 (1980).
[33] L. G. H. Huxley and R. W. Crompton, *The Diffusion and Drift of Electrons in Gases* (Wiley, London, 1974).
[34] R. D. White, R. E. Robson, and K. F. Ness, Appl. Surf. Sci. **192**, 26 (2002).
[35] R. D. White, R. E. Robson, S. Dujko, P. Nicoletopoulos, and B. Li, J. Phys. D **42**, 194001 (2009).
[36] S. Dujko, Z. R. Raspopović, and Z. Lj. Petrović, J. Phys. D **38**, 2952 (2005).
[37] S. Kuhn, Phys. Rev. A **22**, 2460 (1980).
[38] H. R. Skullerud and S. Kuhn, J. Phys. D **16**, 1225 (1983).
[39] U. Becker, R. Dinner, E. Fortunato, J. Kirchner, K. Rosera, and Y. Uchida, Nucl. Instrum. Methods Phys. Res. A **421**, 54 (1999).
[40] E. Fortunato, U. Becker, and R. Dinner, Nucl. Instrum. Methods Phys. Res. A **421**, 278 (1999).
[41] J. J. Kirchner, U. J. Becker, R. B. Dinner, K. J. Fidkowski, and J. H. Wyatt, Nucl. Instrum. Methods Phys. Res. A **474**, 238 (2001).
[42] M. J. Brennan and A. M. Garvie, Aust. J. Phys. **43**, 765 (1990).
[43] K. F. Ness, Phys. Rev. E **47**, 327 (1993).
[44] K. F. Ness, J. Phys. D **27**, 1848 (1994).
[45] R. E. Robson, M. Hildebrandt, and B. Schmidt, Nucl. Instrum. Methods Phys. Res. A **394**, 74 (1997).
[46] X. Bittl, V. Eckardt, H. Fessler, W. G. Gong, M. Konrad, A. Mock, A. Odian, P. Seyboth, J. E. Draper, M. Hildebrandt, K. Ness, and B. Schmidt, Nucl. Instrum. Methods Phys. Res. A **398**, 249 (1997).
[47] R. D. White, K. F. Ness, R. E. Robson, and B. Li, Phys. Rev. E **60**, 2231 (1999).
[48] R. D. White, R. E. Robson, and K. F. Ness, IEEE Trans. Plasma Sci. **27**, 1249 (1999).
[49] R. D. White, K. F. Ness, and R. E. Robson, J. Phys. D **32**, 1842 (1999).
[50] K. Ness and T. Makabe, Phys. Rev. E **62**, 4083 (2000).
[51] D. Loffhagen and R. Winkler, IEEE Trans. Plasma Sci. **27**, 1262 (1999).
[52] B. Li, R. E. Robson, and R. D. White, Phys. Rev. E **74**, 026405 (2006).
[53] P. Nicoletopoulos and R. E. Robson, Phys. Rev. Lett. **100**, 124502 (2008).
[54] R. Winkler, V. A. Maiorov, and F. Sigeneger, J. Appl. Phys. **87**, 2708 (2000).
[55] R. E. Robson, Aust. J. Phys. **47**, 279 (1994).
[56] B. Li, R. D. White, R. E. Robson, and K. F. Ness, Ann. Phys. **292**, 179 (2001).
[57] R. D. White, M. J. Brennan, and K. F. Ness, J. Phys. D **30**, 810 (1997).
[58] Z. M. Raspopović, S. Sakadžić, S. A. Bzenić, and Z. Lj. Petrović, IEEE Trans. Plasma Sci. **27**, 1241 (1999).
[59] S. Dujko, R. D. White, K. F. Ness, Z. Lj. Petrović, and R. E. Robson, J. Phys. D **39**, 4788 (2006).
[60] Z. Lj. Petrović, Z. M. Raspopović, S. Dujko, and T. Makabe, Appl. Surf. Sci. **192**, 1 (2002).
[61] S. Dujko, Ph.D. thesis, James Cook University, 2009.
[62] L. Boltzmann, Wein. Ber. **66**, 275 (1872).
[63] C. S. Wang-Chang, G. E. Uhlenbeck, and J. DeBoer, in *Studies in Statistical Mechanics*, edited by J. DeBoer and G. E. Uhlenbeck (Wiley, New York, 1964), Vol. 2, p. 241.

[64] K. F. Ness and R. E. Robson, Phys. Rev. A **34**, 2185 (1986).
[65] R. E. Robson and K. F. Ness, Phys. Rev. A **33**, 2068 (1986).
[66] R. D. White, R. E. Robson, K. F. Ness, and T. Makabe, J. Phys. D **38**, 997 (2005).
[67] H. R. Skullerud, J. Phys. D **1**, 1567 (1968).
[68] H. Itoh and T. Musha, J. Phys. Soc. Jpn. **15**, 1675 (1960).
[69] S. Dujko, Z. Lj. Petrović, and Z. M. Raspopović (unpublished).
[70] Z. M. Raspopović, S. Dujko, and Z. Lj. Petrović, in *Proceedings of the 17th European Conference on Atomic and Molecular Physics of Ionized Gases* (Constanta, Romania) (2004), p. 47.
[71] A. M. Nolan, M. J. Brennan, K. F. Ness, and A. B. Wedding, J. Phys. D **30**, 2865 (1997).
[72] N. A. Dyatko and A. P. Napartovich, J. Phys. D **32**, 3169 (1999).
[73] L. C. Pitchford, T. J. Moratz, P. Segur, and M. Yousfi, in *Swarm Studies and Inelastic Electron-Molecule Collisions*, edited by L. C. Pitchford, V. B. McCoy, A. Chutjain, and S. Trajmar (Springer-Verlag, New York, 1985), p. 115.
[74] K. Kumar, H. R. Skullerud, and R. E. Robson, Aust. J. Phys. **33**, 343 (1980).
[75] J. Lucas and H. T. Saelee, J. Phys. D **8**, 640 (1975).
[76] Y. Tzeng and E. E. Kunhardt, Phys. Rev. A **34**, 2148 (1986).
[77] K. F. Ness and A. M. Nolan, Aust. J. Phys. **53**, 437 (2000).
[78] R. E. Robson and K. F. Ness, J. Chem. Phys. **89**, 4815 (1988).
[79] S. Bzenić, Z. Lj. Petrović, Z. M. Raspopović, and T. Makabe, Jpn. J. Appl. Phys. **38**, 6077 (1999).
[80] R. E. Robson, R. D. White, and Z. Lj. Petrović, Rev. Mod. Phys. **77**, 1303 (2005).
[81] M. E. Rose, *Elementary Theory of Angular Momentum* (Wiley, New York, 1957).